HHS Public Access

Author manuscript

ACS Appl Nano Mater. Author manuscript; available in PMC 2019 August 24.

Published in final edited form as:

ACS Appl Nano Mater. 2018 August 24; 1(8): 3998–4004. doi:10.1021/acsanm.8b00766.

Opto-Thermophoretic Manipulation and Construction of Colloidal Superstructures in Photocurable Hydrogels

Xiaolei Peng[†,§], **Jingang Li**[†,§], **Linhan Lin**[†,‡,§], **Yaoran Liu**[†], and **Yuebing Zheng**[*,†,‡]

[†]Materials Science & Engineering Program and Texas Materials Institute, The University of Texas at Austin, Austin, Texas 78712, United States

[‡]Department of Mechanical Engineering, The University of Texas at Austin, Austin, Texas 78712, United States

Abstract

Light-based manipulation of colloidal particles holds great promise in fabrication of functional devices. Construction of complex colloidal superstructures using traditional optical tweezers is limited by high operation power and strong heating effect. Herein, we demonstrate low-power opto-thermophoretic manipulation and construction of colloidal superstructures in photocurable hydrogels. By introducing cationic surfactants into a hydrogel solution under a light-directed temperature field, we create both thermoelectric fields and depletion attraction forces to control the suspended colloidal particles. The particles of various sizes and compositions are thus trapped and organized into various superstructures. Furthermore, the colloidal superstructures are immobilized and patterned onto solid-state substrates through UV-induced photopolymerization of the hydrogel. Our opto-thermophoretic technique will open up avenues for bottom-up assembly of colloidal materials and devices.

Graphical Abstract

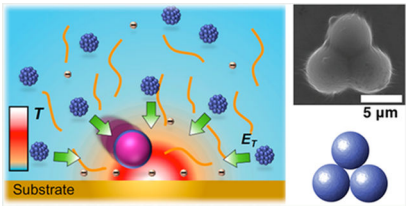

[*]**Corresponding Author:** zheng@austin.utexas.edu.

[§]Author Contributions

X.P., J.L., and L.L. contributed equally to this work. X.P. and Y.Z. conceived the idea. X.P., J.L., and L.L. prepared the materials, worked on the experiments, and collected the data. Y.L. conducted the FDTD simulations. Y.Z. supervised the project. All authors participated in the discussions of the results and wrote the manuscript.

ASSOCIATED CONTENT

Supporting Information

The Supporting Information is available free of charge on the ACS Publications website at DOI: 10.1021/acsanm.8b00766.

Additional figures including parallel trapping and patterning, digital micromirror images, critical CTAC concentration vs PEGD concentration, dark-field scattering spectra, and simulated scattering spectra (PDF)

The authors declare no competing financial interest.

Keywords

thermophoresis; optothermal manipulation; thermoelectric effect; depletion force; colloidal particles; hydrogels

Precise patterning of micro- and nanostructures with complex geometries and configurations is essential for fabrication of functional materials and devices.[1–3] Bottom-up assembly techniques through immobilization and patterning of colloidal particles with precise control of location, spacing, and orientation are particularly promising for the development of functional materials and devices.[4–7] First, colloidal particles as building blocks exhibit precisely tailorable properties down to atomic scale.[8] Second, high-quality crystallinity of colloidal particles from chemical synthesis is retained in the assembly process.[9] Third, assembly of colloidal particles into colloidal matter with precise geometric control will induce collective behaviors beyond what occurs in individual particles.[10,11]

A wide range of techniques have been used to build colloidal superstructures and materials. As a widely applied technique, self-assembly autonomously builds colloidal particles into patterns, which is however often limited to thermodynamically stable colloidal structures.[12] DNA-guided assembly has also been extensively explored to construct programmable particle superlattices, periodic arrays, and asymmetric clusters.[13–16] In particular, the DNA origami technique can create plasmonic nanostructures with precise geometry and position, which can be used for enhanced Raman spectroscopy[17,18] and tunable chiral structures.[19,20]

Optical forces have been explored to pattern colloidal particles into arbitrary superstructures.[21–31] One strategy is to trap and assemble particles into superstructures with optical tweezers and to immobilize the assembled superstructures through van der Waals forces[24,25] or chemical linkages such as photopolymerization.[21,23] Conventional optical tweezers require high power, which may cause irreversible photodamage to the colloidal particles.[32] Optical printing based on plasmon-enhanced optical radiation force is a low-power technique for precise patterning of plasmonic nanoparticles; however, plasmonic heating of already fixed nanoparticles prevents the assembly of particle dimers and clusters in near-field coupling regime.[26,27,30] To overcome this heating obstacle, Stefani's group proposed the use of laser beam that is off-resonance to the plasmon peak wavelength of the printed particles[30] or the use of substrates with high thermal conductivity.[31] Despite all the research efforts, the low-power and versatile optical assembly of colloidal superstructures still remains elusive.

Thermophoresis, which is directed migration of suspended particles under external temperature gradients, has been extensively studied for manipulation of colloidal particles.[33–41] Light-controlled thermophoresis has been judiciously harnessed for low-power optical manipulation of dielectric particles,[42,43] plasmonic nanoparticles,[44] and biological cells.[45] However, most of opto-thermophoretic techniques have been limited to particle manipulation in aqueous solutions with relatively simple compositions. Immobilization of opto-thermophoretically assembled colloidal superstructures for device applications has remained challenging. Herein, we achieve low-power opto-thermophoretic manipulation of colloidal particles in complex hydrogels and further demonstrate the all-optical construction of colloidal superstructures. Specifically, we exploit the micelle-mediated thermoelectric

field and depletion attractive force in a light-controlled temperature field for versatile manipulation and assembly of colloidal particles in photocurable hydrogels. Furthermore, through UV-induced photopolymerization of the hydrogels, we successfully immobilize the assembled colloidal superstructures via the polymer joint. With the low operation power, versatile control, and *in situ* polymerization-based bonding, our optothermophoretic manipulation in hydrogels will find applications in colloidal devices and materials science.

RESULTS AND DISCUSSION

Figure 1a,b illustrates the working principle of optothermophoretic trapping and patterning of a colloidal particle in a photocurable hydrogel. The colloidal particle is suspended in a mixture of cetyltrimethylammonium chloride (CTAC) molecules and photocurable hydrogel, which is sandwiched between a thermoplasmonic substrate and a glass cover slide (see the Materials and Methods section for the details on materials and sample preparation). Above its critical micelle concentration (c_{cmc}: 0.13–0.16 mM), the cationic CTAC surfactant molecules self-assemble into positively charged micelles with a mean radius of 3 nm. CTAC molecules also adsorb on the colloidal particle surface through electrostatic and hydrophobic interactions, leading to a positively charged particle. The hydrogel consists of 10% poly(ethylene glycol) diacrylate (PEGD) 3400 polymers as the cross-linking reagent and 0.05% Irgacure 2959 as the photoinitiator. A temperature gradient is created by irradiating a laser beam onto the thermoplasmonic substrate consisting of a high density of Au nanoparticles, where the excitation of surface plasmons leads to high light-to-heat conversion efficiency. The difference in Soret coefficients between CTAC micelles (also known as macroions) and Cl^- counterions causes the ionic separation. Thus, a localized thermoelectric field E_T is built to trap the positive particle, as shown in Figure 1a. Once the particle is trapped and delivered to a target location, ultraviolet (UV) light is applied to trigger the cross-linking reaction among dispersed PEGD chains and lock the particle onto the substrate, leading to the patterned or immobilized particle (Figure 1b). A real-time process of trapping and patterning a 1 μm polystyrene (PS) bead is shown in Figure 1c and the Supporting Information, Video S1. We have also achieved parallel trapping and patterning of arrays of 1 μm PS beads using a digital micromirror device (DMD) (Figure S1). The optical intensity for the opto-thermophoretic trapping ranges from 0.1 to 0.5 mW/μm^2, which is about 3 orders of magnitude lower than that of optical tweezers.[23,46] With a typical power intensity of 0.2 mW/μm^2, particles can be effectively delivered to the trapping center within a surrounding region of 10 μm in radius.[44]

CTAC surfactant is critical to the low-power opto-thermophoretic manipulation. Meanwhile, the PEGD polymers, the main constituents of the hydrogels, also undergo thermophoresis, which may affect the migration behaviors of colloidal particles in the hydrogel solution. It has been reported that depletion of polymers can lead to accumulation of colloidal particles at the thermal hot spot in colloid−polymer mixtures.[47] To evaluate the contributions of the PEGD polymers and CTAC micelles to the trapping of colloidal particles, we studied the trapping kinetics of a single 500 nm PS sphere under a light-controlled temperature field in a pure hydrogel solution (Figure 2a,b) and a hydrogel solution of 10 mM CTAC (Figure 2c,d), respectively. Both solutions were confined in a 20 μm thin chamber to suppress the thermal convection and to rule out the thermofluidic effect on the colloidal dynamics.[48] The real-

time trajectories of colloidal particles under the temperature field were recorded with a fast CCD camera. Under a temperature gradient ∇T with a magnitude of ~10 K/μm,[44] the 500 nm PS bead in the pure hydrogel solution underwent Brownian motion without significant confinement by the laser spot, as shown in Figure 2b (also see the Supporting Information, Video S2). It implies the depletion force arising from the 10% PEGD polymers was too weak to overcome the Brownian motion of the particle for its stable trapping.

In contrast, the PS bead was stably trapped in the hydrogel solution with 10 mM CTAC, as shown in Figure 2d (also see the Supporting Information, Video S2). It should be noted that the temperature gradient ∇T is barely changed when introducing the CTAC into the hydrogel solution, for ∇T is determined by the heat transfer between the Au substrate and the hydrogel solution. Under the temperature gradient ∇T (~10 K/μm), both the CTAC micelles and Cl^- ions migrate from the hot to cold region with a drift velocity given by $\boldsymbol{u} = D_T \nabla T$, where D_T is the thermophoretic mobility. When it comes to steady state, a concentration gradient forms in the temperature field, i.e., $\nabla c = -S_T c \nabla T$, where c is the micelle or ion concentration, and $S_T = D_T/D$ (D is the diffusion coefficient) is the corresponding Soret coefficient. Due to a much larger Soret coefficient of the CTAC micelles (~10^{-2} K^{-1}) than that of the Cl^- ions (~7.18×10^{-4} K^{-1}), the spatially redistributed CTAC micelles and Cl^- ions generate the thermoelectric field E_T that directs the positively charged PS beads along the temperature gradient, i.e., from the cold to hot region. Trapping of the beads is achieved at the laser spot with the balanced thermoelectric force and repulsive electro-static force from the substrate. The substrate is also positively charged due to the coating of CTAC double layers.[49] To estimate the trapping stability, we conducted Gaussian fitting for the histogram of the particle displacements, which gives a variance σ of ~15 nm in both the x and y directions, corresponding to a trapping stiffness κ of ~37 pN/μm $\left(\kappa = \frac{2k_B T}{\sigma^2}\right)$. To generate the same trapping stiffness for a 500 nm PS sphere, optical tweezers typically require a power of ~100 mW,[23,46] which is 3 orders of magnitude higher than the working power (0.23 mW) of our opto-thermophoretic tweezers.

Besides the opto-thermoelectric field from the thermophoretic migration of CTAC micelles and Cl^- ions, the interaction between the CTAC surfactant and the PEGD polymers should also be considered for the trapping behaviors of colloidal particles. Specifically, the association or binding of the CTAC micelles to the PEGD polymers, which scales linearly with the polymer concentration,[50] can significantly screen the thermo-electric field and increase the critical CTAC concentration for efficient opto-thermophoretic trapping. In the 10% PEGD polymer solution, which is typically the lowest concentration for UV cross-linking, we obtained a minimum CTAC concentration of 2 mM for trapping, which is 1 order of magnitude higher than that in aqueous solutions without hydrogels (Figure S2). When the CTAC concentration increases from 2 to 20 mM, the association effect becomes saturated, and the amount of free-form CTAC micelles increases linearly. It should be noted that the thermophoresis of CTAC micelles also introduces a depletion force between the particle and the substrate, which improves the trapping stiffness at high CTAC concentration. To verify our hypothesis, we measured the trapping stiffness of single 500 nm PS beads as a function of CTAC concentration from 2 to 20 mM (Figure 2e). The trapping stiffness

increases rapidly with the CTAC concentration in the range 2−10 mM because of the enhanced particle−substrate depletion attraction and becomes relatively constant in the range 10−20 mM. The trapping stiffness at 20 mM CTAC is improved by 1 order of magnitude because of the dominant depletion force.[44]

It is essential for a fabrication technique to pattern colloidal particles of various sizes and compositions while retaining their intrinsic physical properties. We have further integrated a high-performance spectrometer into our tweezers to carry out *in situ* dark-field optical spectroscopy of the patterned particles, which include high-refractive-index silicon nanospheres (SiNSs) and plasmonic gold nanospheres (AuNSs). Figure 3a shows the scattering spectra of a single 300 nm SiNS trapped in the hydrogel near the substrate (blue curve) and patterned onto the substrate after UV-induced cross-linking of the hydrogel (red curve). Two scattering peaks emerge at 675 and 765 nm, which correspond to the electric quadrupole and magnetic quadrupole due to Mie resonance of the SiNS, respectively.[51] No obvious change in the spectra of a 300 nm SiNS (Figure 3a) and a 500 nm SiNS (Figure S3) after the patterning indicates the cross-linking process does not change the surroundings' refractive index or the particles themselves. We have further demonstrated the patterning of 100 nm AuNS dimers that support the near-field coupling. As shown in Figure 3b, the scattering peak (580 ± 10 nm) of a single AuNS splits into two peaks when two AuNSs are trapped and patterned in a hydrogel solution of 20 mM CTAC. Our finite-difference time-domain (FDTD) simulation reveals that the two peaks correspond to a longitudinal mode (636 nm) and a transverse mode (570 nm) of the coupled AuNS dimer with a gap of ~30 nm (see Figure S4a). Repeated measurements of various AuNS dimers show that the longitudinal mode spans the range 636 ± 10 nm, which represents a gap distance of 25−50 nm (see Figure S4b). The capability of patterning nanoparticles at the near-field coupling distance enables the construction of complex architectures with emerging properties.

We have applied the opto-thermophoretic manipulation and patterning to build diverse colloidal superstructures with colloidal particles of various sizes, dimensions and compositions. The interparticle depletion attraction interaction acts as the major "bonding" force to assemble the superstructures in hydrogels,[42] which are further immobilized via photopolymerization. Figure 4a–c shows two-dimensional (2D) close-packed colloidal superstructures of 1, 2, and 5 μm PS spheres, respectively. It is worth noting that the as-built superstructures remained intact even after the samples were rinsed and dried. The scanning electron micrograph in Figure 4c shows the superstructure was joined by photocured hydrogels. Figure 4d shows a one-dimensional (1D) chain of 2 μm PS spheres. Figure 4e shows a 2D Saturn-ring structure consisting of a 5 μm PS sphere surrounded by eight 2 μm PS spheres. By further incorporating optical scattering force into the opto-thermophoretic system, we achieve out-of-plane manipulations to build three-dimensional (3D) superstructures. As an example, we show a 3D tetrahedron superstructure with four 2 μm PS spheres (Figure 4f). To demonstrate the capability of building hybrid colloidal superstructures with particles of different compositions and sizes, we manage to arrange two 5 μm PS spheres and two 2 μm silica particles into two types of configurations (Figure 4g,h). Figure 4i,j shows that three PS spheres with different sizes are arranged into left-handed or right-handed chiral configurations.

CONCLUSIONS

Exploiting micelle-mediated opto-thermoelectric fields for colloidal manipulation in hydrogels and UV-induced photo-polymerization of the hydrogels, we have developed an optothermophoretic patterning technique for versatile assembly of colloidal particles onto solid-state substrates. It is revealed that thermophoresis of the CTAC micelles, particle −substrate and particle−particle depletion attraction, and the micelle− polymer bonding contribute to the opto-thermophoretic trapping. The trapping efficiency can be optimized by tuning the CTAC concentration, and a trapping stiffness of tens of pN/μm can be achieved for submicron colloidal particles. Using colloidal particles in a wide range of sizes and compositions as the building blocks, we demonstrate the assembly of complex colloidal superstructures with diverse configurations. Integrating *in situ* spectroscopic analysis into the opto-thermophoretic system, we can study the responses of colloidal superstructures to light fields. With its versatile, low-power, and noninvasive operation, the opto-thermophoretic patterning strategy will find applications in studies of light−matter interactions and nanofabrication of colloidal devices.

MATERIALS AND METHODS

Materials and Sample Preparation.

Thermoplasmonic substrates were prepared by depositing Au thin films on glass coverslips with thermal deposition (Denton thermal evaporator; base pressure, 1×10^{-5} Torr) followed by thermal annealing at 550 °C for 2 h. The thermal annealing leads to the formation of quasicontinuous Au nanoislands. Au films of 4.5 and 6.5 nm were deposited and annealed to match with a 532 and 660 nm laser wavelength, respectively. PS spheres and silica spheres were purchased from Bangs Laboratories Inc. AuNSs were purchased from Nano Composix. SiNSs were synthesized with a previously reported method.[51] CTAC, poly-(ethylene glycol) diacrylate (PEGD) 3400 polymers, and Irgacure 2959 photoinitiator were purchased from Chem-Impex, Alfa Aesar, and Sigma-Aldrich, respectively. The colloidal particles were diluted to from 5×10^5 to 5×10^6 particles/mL and then added to hydrogel solutions containing 10% PEGD 3400 polymers as the cross-linking reagent, 0.05% Irgacure 2959 as the photoinitiator, and 2−20 mM CTAC for trapping and assembly experiments. The scanning electron micrographs were taken using an FEI Quanta 650 ESEM instrument.

Optical Setup.

A 532 nm diode-pumped solid-state laser (Genesis MX STM-1 W; Coherent) was expanded with a 5× beam expander (Thorlabs, GBE05-A) and projected onto a digital micromirror device (DMD). Optical patterns reflected from the DMD were focused onto the substrates by a 40× objective (Nikon, NA 0.75) in an inverted microscope (Nikon Ti-E). For trapping stiffness measurement, the DMD and related setup were removed, and a 100× oil objective (Nikon, NA 0.5–1.3) was used. A color CCD camera (Nikon) and a fast monochromic CCD camera (Andor) were used to record optical images and to measure the trapping stiffness, respectively. A 533 nm notch filter was inserted between the objective and the cameras to block the laser beam. For the trapping stiffness measurement in Figure 2, a 660 nm diode-pumped solid-state laser (Opus 660 1.5W; Laser quantum) was expanded with a 10× beam

expander and focused by the 100× oil objective. A 658 nm notch filter was inserted between the objective and the cameras to block the laser beam.

FDTD Simulations.

Scattering spectra of metal nanoparticles were simulated using FDTD methods (Lumerical FDTD solutions). A refractive index of 1.52 was set for the glass substrate. A mesh size of 1 nm was applied to define the metal nanoparticles. Frequency domain field profile monitors were applied to calculate the *E*-field distributions and the scattering spectra of particles embedded in water medium ($n = 1.33$).

Supplementary Material

Refer to Web version on PubMed Central for supplementary material.

ACKNOWLEDGMENTS

The authors acknowledge the financial support of the Army Research Office (W911NF-17–1-0561) and the National Institute of General Medical Sciences of the National Institutes of Health (DP2GM128446). We thank Taizhi Jiang and Brian A. Korgel from the Department of Chemical Engineering at UT Austin for providing silicon nanoparticles. We also thank the Texas Advanced Computing Center at The University of Texas at Austin for providing HPC resources that have contributed to the research results reported within this paper (URL: http://www.tacc.utexas.edu).

REFERENCES

(1). Gates BD; Xu Q; Love JC; Wolfe DB; Whitesides GM Unconventional Nanofabrication. Annu. Rev. Mater. Res 2004, 34, 339–372.

(2). Gates BD; Xu Q; Stewart M; Ryan D; Willson CG; Whitesides GM New Approaches to Nanofabrication: Molding, Printing, and Other Techniques. Chem. Rev 2005, 105, 1171–1196. [PubMed: 15826012]

(3). Quake SR; Scherer A From Micro- to Nanofabrication with Soft Materials. Science 2000, 290, 1536–1540. [PubMed: 11090344]

(4). Shimomura M; Sawadaishi T Bottom-up Strategy of Materials Fabrication: A New Trend in Nanotechnology of Soft Materials. Curr. Opin. Colloid Interface Sci 2001, 6, 11–16.

(5). Durham JW; Zhu Y Fabrication of Functional Nanowire Devices on Unconventional Substrates Using Strain-Release Assembly. ACS Appl. Mater. Interfaces 2013, 5, 256–261. [PubMed: 23249184]

(6). Wu Y; Dong N; Fu S; Fowlkes JD; Kondic L; Vincenti MA; de Ceglia D; Rack PD Directed Liquid Phase Assembly of Highly Ordered Metallic Nanoparticle Arrays. ACS Appl. Mater. Interfaces 2014, 6, 5835–5843. [PubMed: 24689648]

(7). Liu T; Keiper T; Wang X; Yang G; Hallinan D; Zhao J; Xiong P Molecular Patterning and Directed Self-Assembly of Gold Nanoparticles on GaAs. ACS Appl. Mater. Interfaces 2017, 9, 43363–43369. [PubMed: 29140682]

(8). Yang S-M; Kim S-H; Lim J-M; Yi G-R Synthesis and Assembly of Structured Colloidal Particles. J. Mater. Chem 2008, 18, 2177–2190.

(9). Kuai S-L; Hu X-F; Haché A; Truong V-V High-Quality Colloidal Photonic Crystals Obtained by Optimizing Growth Parameters in a Vertical Deposition Technique. J. Cryst. Growth 2004, 267, 317–324.

(10). Velev OD; Kaler EW In Situ Assembly of Colloidal Particles into Miniaturized Biosensors. Langmuir 1999, 15, 3693–3698.

(11). Hynninen A-P; Thijssen JHJ; Vermolen ECM; Dijkstra M; van Blaaderen A Self-Assembly Route for Photonic Crystals with a Bandgap in the Visible Region. Nat. Mater 2007, 6, 202–205. [PubMed: 17293851]

(12). Whitesides GM; Grzybowski B Self-Assembly at All Scales. Science 2002, 295, 2418–2421. [PubMed: 11923529]

(13). Tian Y; Wang T; Liu W; Xin HL; Li H; Ke Y; Shih WM; Gang O Prescribed Nanoparticle Cluster Architectures and Low- Dimensional Arrays Built Using Octahedral DNA Origami Frames. Nat. Nanotechnol 2015, 10, 637–644. [PubMed: 26005999]

(14). Gang O; Tkachenko AV DNA-Programmable Particle Superlattices: Assembly, Phases, and Dynamic Control. MRS Bull. 2016, 41, 381–387.

(15). Lin Q-Y; Mason JA; Li Z; Zhou W; O'Brien MN; Brown KA; Jones MR; Butun S; Lee B; Dravid VP; Aydin K; Mirkin CA Building Superlattices from Individual Nanoparticles via Template-Confined DNA-Mediated Assembly. Science 2018, 359, 669–672. [PubMed: 29348364]

(16). Schade NB; Holmes-Cerfon MC; Chen ER; Aronzon D; Collins JW; Fan JA; Capasso F; Manoharan VN Tetrahedral Colloidal Clusters from Random Parking of Bidisperse Spheres. Phys. Rev. Lett 2013, 110, 148303. [PubMed: 25167045]

(17). Thacker VV; Herrmann LO; Sigle DO; Zhang T; Liedl T; Baumberg JJ; Keyser UF DNA Origami Based Assembly of Gold Nanoparticle Dimers for Surface-Enhanced Raman Scattering. Nat. Commun 2014, 5, 3448. [PubMed: 24622339]

(18). Kühler P; Roller E-M; Schreiber R; Liedl T; Lohmüller T; Feldmann J Plasmonic DNA-Origami Nanoantennas for Surface-Enhanced Raman Spectroscopy. Nano Lett. 2014, 14, 2914–2919. [PubMed: 24754830]

(19). Kuzyk A; Schreiber R; Fan Z; Pardatscher G; Roller E-M; Högele A; Simmel FC; Govorov AO; Liedl T DNA-Based Self-Assembly of Chiral Plasmonic Nanostructures with Tailored Optical Response. Nature 2012, 483, 311. [PubMed: 22422265]

(20). Shen X; Asenjo-Garcia A; Liu Q; Jiang Q; García de Abajo FJ; Liu N; Ding B Three-Dimensional Plasmonic Chiral Tetramers Assembled by DNA Origami. Nano Lett. 2013, 13, 2128–2133. [PubMed: 23600476]

(21). Mio C; Marr DWM Optical Trapping for the Manipulation of Colloidal Particles. Adv. Mater 2000, 12, 917–920.

(22). Urban AS; Carretero-Palacios S; Lutich AA; Lohmuller T; Feldmann J; Jackel F Optical Trapping and Manipulation of Plasmonic Nanoparticles: Fundamentals, Applications, and Perspectives. Nanoscale 2014, 6, 4458–4474. [PubMed: 24664273]

(23). Shaw LA; Chizari S; Panas RM; Shusteff M; Spadaccini CM; Hopkins JB Holographic Optical Assembly and Photo-polymerized Joining of Planar Microspheres. Opt. Lett 2016, 41, 3571–3574. [PubMed: 27472621]

(24). Guffey MJ; Scherer NF All-Optical Patterning of Au Nanoparticles on Surfaces Using Optical Traps. Nano Lett. 2010, 10, 4302–4308. [PubMed: 20925400]

(25). Bao Y; Yan Z; Scherer NF Optical Printing of Electrodynamically Coupled Metallic Nanoparticle Arrays. J. Phys. Chem. C 2014, 118, 19315–19321.

(26). Nedev S; Urban AS; Lutich AA; Feldmann J Optical Force Stamping Lithography. Nano Lett. 2011, 11, 5066–5070. [PubMed: 21992538]

(27). Do J; Fedoruk M; Jäckel F; Feldmann J Two-Color Laser Printing of Individual Gold Nanorods. Nano Lett. 2013, 13, 4164–4168. [PubMed: 23927535]

(28). Roxworthy BJ; Ko KD; Kumar A; Fung KH; Chow EKC; Liu GL; Fang NX; Toussaint KC Application of Plasmonic Bowtie Nanoantenna Arrays for Optical Trapping, Stacking, and Sorting. Nano Lett. 2012, 12, 796–801. [PubMed: 22208881]

(29). Ndukaife JC; Kildishev AV; Nnanna AGA; Shalaev VM; Wereley ST; Boltasseva A Long-Range and Rapid Transport of Individual Nano-Objects by a Hybrid Electrothermoplasmonic Nanotweezer. Nat. Nanotechnol 2015, 11, 53. [PubMed: 26524398]

(30). Gargiulo J; Cerrota S; Cortés E; Violi IL; Stefani FD Connecting Metallic Nanoparticles by Optical Printing. Nano Lett. 2016, 16, 1224–1229. [PubMed: 26745330]

(31). Gargiulo J; Brick T; Violi IL; Herrera FC; Shibanuma T; Albella P; Requejo FG; Cortes E; Maier SA; Stefani FD Understanding and Reducing Photothermal Forces for the Fabrication of Au Nanoparticle Dimers by Optical Printing. Nano Lett. 2017, 17, 5747–5755. [PubMed: 28806511]

(32). González-Rubio G; Guerrero-Martínez A; Liz-Marzán LM Reshaping, Fragmentation, and Assembly of Gold Nanoparticles Assisted by Pulse Lasers. Acc. Chem. Res 2016, 49, 678–686. [PubMed: 27035211]

(33). Piazza R Thermophoresis: Moving Particles with Thermal Gradients. Soft Matter 2008, 4, 1740–1744.

(34). Wurger A Thermal Non-Equilibrium Transport in Colloids. Rep. Prog. Phys 2010, 73, 126601.

(35). Chen J; Kang Z; Kong SK; Ho H-P Plasmonic Random Nanostructures on Fiber Tip for Trapping Live Cells and Colloidal Particles. Opt. Lett 2015, 40, 3926–3929. [PubMed: 26368677]

(36). Kang Z; Chen J; Wu S-Y; Chen K; Kong S-K; Yong K-T; Ho H-P Trapping and Assembling of Particles and Live Cells on Large-Scale Random Gold Nano-Island Substrates. Sci. Rep 2015, 5, 9978. [PubMed: 25928045]

(37). Ly A; Majee A; Wurger A Nanoscale Seebeck Effect at Hot Metal Nanostructures. New J. Phys 2018, 20, 025001.

(38). Talbot EL; Kotar J; Parolini L; Di Michele L; Cicuta P Thermophoretic Migration of Vesicles Depends on Mean Temperature and Head Group Chemistry. Nat. Commun 2017, 8, 15351. [PubMed: 28513597]

(39). Smith CLC; Thilsted AH; Pedersen JN; Youngman TH; Dyrnum JC; Michaelsen NA; Marie R; Kristensen A Photothermal Transport of DNA in Entropy-Landscape Plasmonic Waveguides. ACS Nano 2017, 11, 4553–4563. [PubMed: 28453288]

(40). Reichl MR; Braun D Thermophoretic Manipulation of Molecules inside Living Cells. J. Am. Chem. Soc 2014, 136, 15955–15960. [PubMed: 25171388]

(41). Reichl M; Herzog M; Götz A; Braun D Why Charged Molecules Move across a Temperature Gradient: The Role of Electric Fields. Phys. Rev. Lett 2014, 112, 198101. [PubMed: 24877967]

(42). Lin L; Zhang J; Peng X; Wu Z; Coughlan ACH; Mao Z; Bevan MA; Zheng Y Opto-Thermophoretic Assembly of Colloidal Matter. Sci. Adv 2017, 3, e1700458. [PubMed: 28913423]

(43). Lin L; Peng X; Mao Z; Wei X; Xie C; Zheng Y Interfacial-Entropy-Driven Thermophoretic Tweezers. Lab Chip 2017, 17, 3061–3070. [PubMed: 28805878]

(44). Lin L; Wang M; Peng X; Lissek EN; Mao Z; Scarabelli L; Adkins E; Coskun S; Unalan HE; Korgel BA; Liz-Marzán LM; Florin E-L; Zheng Y Opto-Thermoelectric Nanotweezers. Nat. Photonics 2018, 12, 195–201. [PubMed: 29785202]

(45). Lin L; Peng X; Wei X; Mao Z; Xie C; Zheng Y Thermophoretic Tweezers for Low-Power and Versatile Manipulation of Biological Cells. ACS Nano 2017, 11, 3147–3154. [PubMed: 28230355]

(46). Neuman KC; Block SM Optical Trapping. Rev. Sci. Instrum 2004, 75, 2787–2809. [PubMed: 16878180]

(47). Jiang H-R; Wada H; Yoshinaga N; Sano M Manipulation of Colloids by a Nonequilibrium Depletion Force in a Temperature Gradient. Phys. Rev. Lett 2009, 102, 208301. [PubMed: 19519079]

(48). Roxworthy BJ; Bhuiya AM; Vanka SP; Toussaint KC Jr, Understanding and Controlling Plasmon-Induced Convection. Nat. Commun 2014, 5, 3173. [PubMed: 24445431]

(49). Gómez-Graña S; Hubert F; Testard F; Guerrero-Martínez A; Grillo I; Liz-Marzán LM; Spalla O Surfactant (Bi)Layers on Gold Nanorods. Langmuir 2012, 28, 1453–1459. [PubMed: 22165910]

(50). Holmberg K; Jönsson B; Kronberg B; Lindman B Surfactants and Polymers in Aqueous Solution; Wiley: Chichester, 2003; Chapter 13, pp 277–303.

(51). Shi L; Harris JT; Fenollosa R; Rodriguez I; Lu X; Korgel BA; Meseguer F Monodisperse Silicon Nanocavities and Photonic Crystals with Magnetic Response in the Optical Region. Nat. Commun 2013, 4, 1904. [PubMed: 23695698]

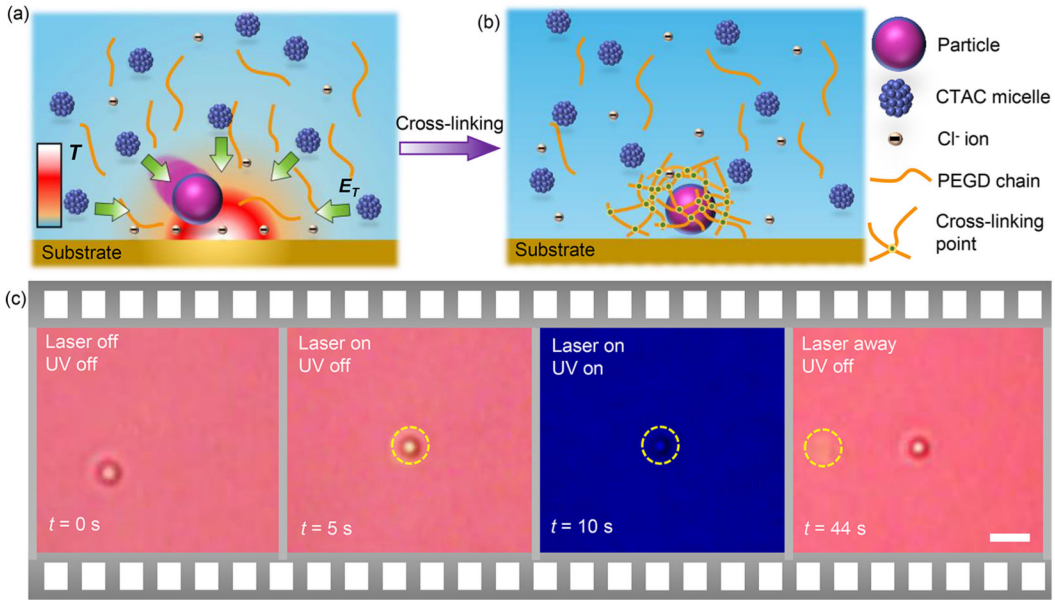

Figure 1.

Opto-thermophoretic trapping and patterning of a colloidal particle in a hydrogel solution. (a) Schematic illustration of trapping of a colloidal particle in a thermoelectric field induced by the thermophoretic separation of dispersed CTAC micelles and Cl^- ions. (b) Schematic illustration of immobilization and patterning of the trapped colloidal particle through UV cross-linking. (c) Sequential optical images of trapping and patterning of a 1 μm PS sphere in a hydrogel solution with 20 mM CTAC. The thermoplasmonic substrate in parts a and b represents a quasicontinuous film consisting of a high density of Au nanoparticles. A 532 nm laser beam with a diameter of 2 μm and an optical intensity of 0.3 mW/μm^2 was used for opto-thermophoretic trapping. The laser beam is indicated by dashed circles in part *c*. Scale bar in part c: 2 μm.

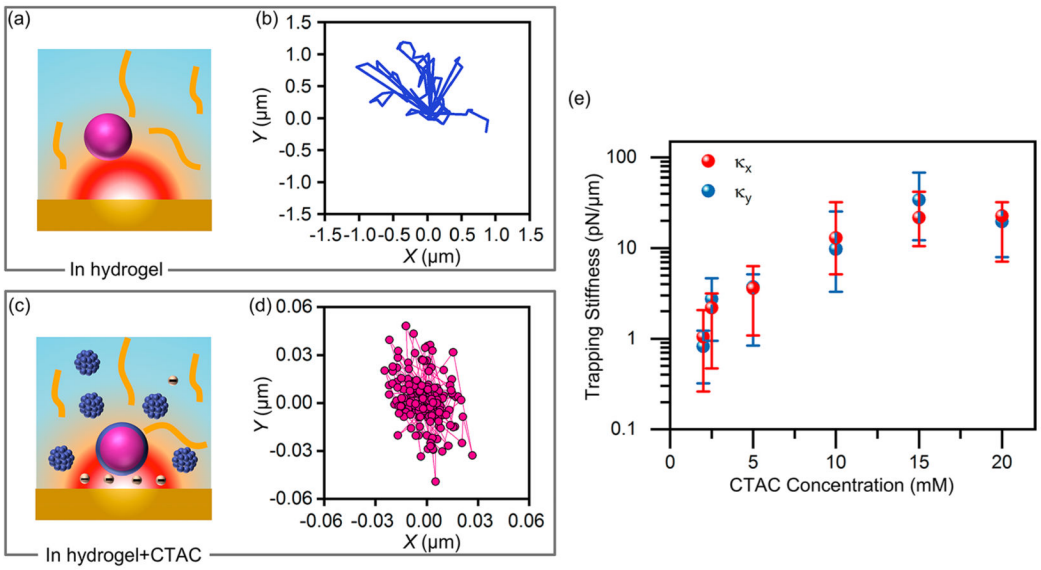

Figure 2.

Effect of CTAC concentration on opto-thermophoretic trapping of colloidal particles. (a) Schematic illustration and (b) time trace of a 500 nm PS sphere under an optically controlled temperature field in a pure hydrogel solution. (c) Schematic illustration and (d) time trace of a 500 nm PS sphere under an optically controlled temperature field in a hydrogel solution with 10 mM CTAC. (e) Trapping stiffness for 500 nm PS spheres as a function of CTAC concentration. κ_x and κ_y are the trapping stiffness in the x and y directions, respectively. The error bars represent the deviation in five measurements with different particles. A (a–d) 20 μm and (e) 120 μm thick spacer were used to confine the solutions between a Au substrate and a coverslip, respectively. A 660 nm laser beam with a diameter of 943 nm and an optical power of 0.23 mW was irradiated onto the Au substrate.

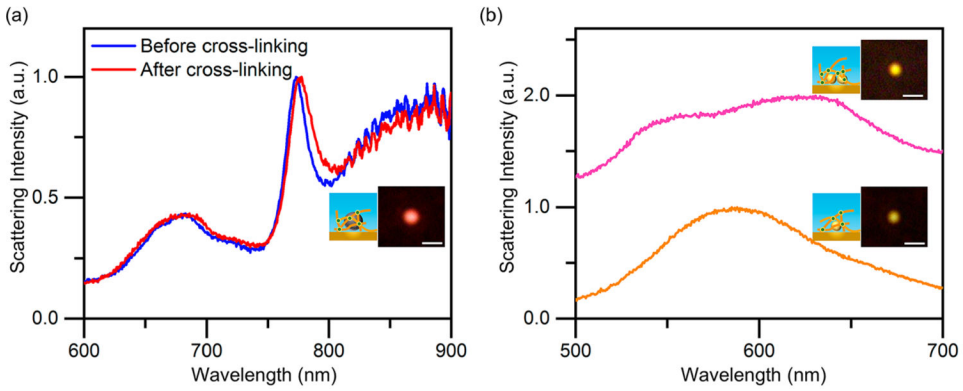

Figure 3.

Optical spectroscopy of trapped and patterned nanoparticles in hydrogel solutions. (a) Dark-field scattering spectra of a 300 nm SiNS before and after cross-linking. (b) Dark-field scattering spectra of a single AuNS (bottom) and two AuNSs as a dimer (top) after cross-linking. The insets show the schematic illustrations and dark-field optical images for each curve after cross-linking. A 532 nm laser beam with a diameter of ~520 nm and a power intensity of 0.2 mW/μm^2 was used to trap the particles in a hydrogel solution of 20 mM CTAC. Scale bars in the insets of parts a and b: 1 μm.

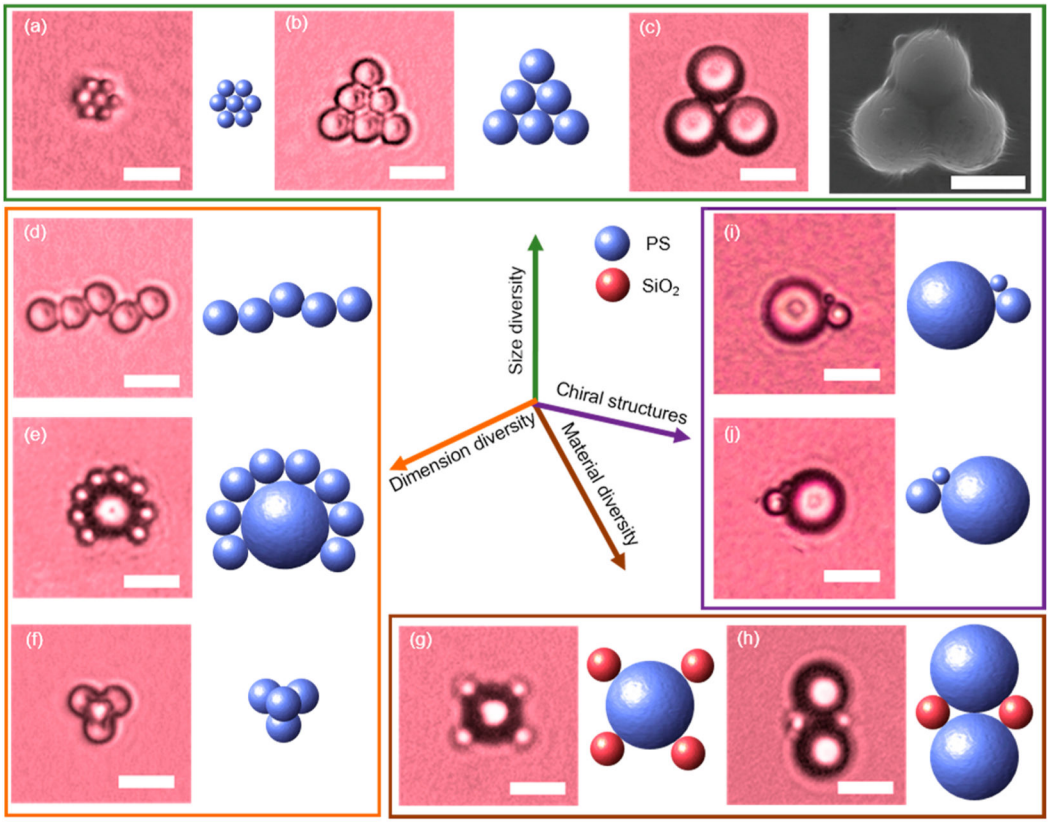

Figure 4.

Opto-thermophoretic assembly and immobilization of various colloidal superstructures in hydrogel solutions. Assembly of (a) 1, (b) 2, and (c) 5 μm PS spheres into 2D close-packed superstructures. (d) 1D assembly of 2 μm PS spheres. (e) 2D hybrid assembly of a Saturn-ring superstructure with a 5 μm PS sphere and eight 2 μm PS spheres. (f) 3D assembly of a close-packed tetrahedron superstructure with four 2 μm PS spheres. (g) 2D hybrid assembly of a 5 μm PS sphere surrounded with four 2 μm silica spheres. (h) 2D hybrid assembly of two 5 μm PS spheres and two 2 μm silica spheres. (i, j) 2D hybrid assembly of a 1, 2, and 5 μm PS sphere into two close-packed superstructures with an opposite chirality. The pink images are the corresponding optical microscopy images. The inset in part *c* shows the scanning electron micrograph of the corresponding superstructure after cross-linking of the hydrogel. All the colloidal superstructures were assembled in hydrogel solutions of 20 mM CTAC and patterned via UV-induced cross-linking. For assembly, 20 mM is an optimized concentration for strong depletion attraction between the assembled particles. A 532 nm laser beam with a diameter of 2 μm was used for assembly. Scale bars: 5 μm.